WILEY | Hindawi

Research Article

Influence of the Volute Tongue Shape on Cavitation Performance in Aviation Fuel Centrifugal Pump

Siwei Zhao [ID],[1] **Yiming Li,**[2] **Ling Zhang,**[2] **Kai Wang** [ID],[1,2] **and Guangzhao Luo**[3]

[1]*Research Center of Fluid Machinery Engineering and Technology, Jiangsu University, Zhenjiang 212013, China*
[2]*Xinxiang Aviation Industry (Group) Co., Ltd., Xinxiang 453003, China*
[3]*Xi'an Aerospace Propulsion Institute, Xi'an 710199, China*

Correspondence should be addressed to Kai Wang; wangkai@ujs.edu.cn

During the operation of an aviation fuel centrifugal pump, the performance of the pump dropped sharply due to cavitation, which caused cavitation damage near the volute tongue, which seriously threatened the safe and stable operation of the aircraft. According to the characteristics that the cavitation in the volute tongue region occurs in large flow rate, the volute tongue shape of aviation fuel centrifugal pump was improved in this paper, and the influence of the volute tongue shape on the cavitation characteristics of aviation fuel centrifugal pump at 1.2 times of design flow rate was studied. The research shows that under 1.2 times of design flow rate, the critical cavitation number of the improved volute tongue shape is reduced by 7.4% compared with the original scheme. The improved volute tongue effectively suppresses the generation of cavitation in the volute tongue region. The vortex core distribution area is reduced compared to the original scheme. When the cavitation number is low, doubling the axial passing frequency on the pressure pulsation spectrum at the monitoring point of the volute tongue is obviously weakened.

1. Introduction

An aviation fuel pump is an important component of the aircraft fuel system. Its function is mainly to transport all kinds of aviation fuel and to provide flow rate and pressure for aviation engines and fuel systems. With the rapid development of modern aerospace science and technology, the performance requirements of a fuel pump are gradually improved [1]. The working performance and reliability of the fuel centrifugal pump will affect the safe and stable operation of the aircraft. As the aircraft usually operates in various extreme and harsh environments, cavitation of the fuel pump is more serious, which causes cavitation damage to flow passage components, affects the stable fuel supply performance of the fuel pump, and has a serious impact on the safe and stable operation of the aircraft.

With the rapid development of CFD, it is more convenient to study the cavitation problem in the fuel pump. Kim et al. [2] improved the prediction of accuracy about the generation of cavitation and development by using tran-sient simulation and analysis of the numerical simulation. Wang et al. [3] studied the characteristics of irreversible energy loss caused by cavitation flow in a centrifugal pump and employed the entropy production theory with CFD to analyze the relationship between flow field details of cavitation flow and irreversible flow loss. Zhu et al. [4] proposed the density-corrected RNG k-ε model for cavitation simulation and used three different cavitation erosion prediction methods to predict cavitation erosion on the blade surface of the centrifugal pump. Zhang et al. [5] studied the influence of opening at the blade inlet on the cavitation performance of a centrifugal pump based on the Rayleigh-Plesset cavitation model. The research showed that the opening structure can not only suppress the generation of cavitation but also reduced the turbulent kinetic energy loss and improved the overall performance of the centrifugal pump. Mousmouli et al. [6] studied the influence of blade tip clearance and thickness on the performance of the centrifugal pump and verified the reliability of numerical simulation by using experimental data. The research results showed that

the prediction accuracy of the Zwart model was relatively high. Zhao et al. [7] studied the influence of the Zwart model on the cavitation performance of aviation fuel pump by using alternative fuel and optimized the structural parameters of the inducer and impeller by using the surrogate model, which significantly improved the overall performance of fuel centrifugal pump. Wang [8] studied the cavitation performance of an aviation fuel pump and found that cavitation caused the unsteady change of fuel pump load, which caused more serious damage to the blade. At the same time, the interaction between the blades of the fuel pump made the cavitation in the blade flow passage show the characteristics of the asymmetric structure. Hu et al. [9] optimized the design of a centrifugal fire pump with a specific speed of 24.7 and made numerical calculations and experiment measurements to obtain the best optimized scheme. Results showed that compared with the original scheme, the critical net positive suction head of the best optimized scheme was reduced by 21.5%, 17.6%, 15.7%, and 16.8%, respectively. Wang et al. [10] analyzed the effect of cavitation on the vibration of a five-stage centrifugal pump under noncavitation and cavitation conditions. In addition, for the energy loss caused by cavitation, Liu et al. [11] took the hydrofoil as the research object and analyzed that the separation of the sheet cavity and the shedding of the cloud cavity induced the generation of multiscale vortical structures, which significantly increased the energy loss. Chen et al. [12] used the improved cavitation model to study the energy loss inside the inducer, which can take the tip leakage as a key parameter to reduce the occurrence of thermal cavitation in the liquid nitrogen inducer and provide a reference for the design of the inducer. Li et al. [13, 14] studied the relationship between cavitation region and entropy generation by using of local flow analysis method and analyzed the influence of vortex evolution on flow instability.

In the hydraulic design process of a fuel centrifugal pump, the structure size and processing technology of flow passage components will affect the internal cavitation performance of the fuel pump. Scholars around the world have done a lot of research on the influence of geometric structure on the cavitation performance of the centrifugal pump. Visser [15] designed a new combination of impeller and volute. Through experimental verification, it was found that the cavitation at the leading edge of the impeller was significantly weakened and the efficiency increased. Schiavello and Visser [16] studied the cavitation of the pump and proposed a characterization index to judge the degree of cavitation by using of 3% head drop, 40000-hour impeller life, and cavitation residual heat scale law. Li et al. [17] studied different cavitation types and the unsteady process of cavitation motion based on the inlet deflection angle of the inducer. The research showed that a reasonable blade inlet deflection angle can achieve better cavitation performance. Wang et al. [18] optimized the design of a fuel centrifugal pump based on the SAP optimization algorithm, which made the internal flow of the centrifugal pump more stable. Dupont [19] studied the influence law of long, medium, and short composite blades on the unsteady characteristics of fuel centrifugal pump under low flow rates. Through experimental verifica-

tion, the efficiency has been improved. Li et al. [20] conducted the numerical simulation and experiment of an aerofuel centrifugal pump with a combination impeller and analyzed the effect of a combination impeller on the flow field and external performance of the aerofuel centrifugal pump.

However, nowadays, researches about the cavitation performance of aviation fuel centrifugal pumps are still insufficient. Therefore, this paper is aimed at the cavitation problem in the volute tongue region of the fuel centrifugal pump and combines its characteristics under 1.2 times of design flow rate, to study the influence of improved volute tongue shape on the cavitation performance of the fuel centrifugal pump, in order to weaken the cavitation damage in the volute tongue region.

2. Research Model

2.1. Original Model. The computational domain of the aviation fuel pump used in this paper includes the inlet extension, valve runner, impeller, volute, outlet elbow, and outlet extension (as shown in Figure 1). Its design parameters are the rotational speed which is 26400 r/min and the number of the blade which is 6.

2.2. Improved Scheme. The fuel centrifugal pump was operated continuously for 50 hours at different cavitation numbers, and the cavitation damage was very serious near the volute tongue, as shown in Figure 2. Therefore, it is necessary to improve the structure of the volute tongue in order to improve the cavitation performance of the fuel pump and weaken the cavitation damage caused by cavitation.

In the original scheme, the contour line of the volute tongue is not parallel to the axis; its shape is that the annular cavity of the volute intersects with the diffusion section to form an intersecting line. Therefore, the shape of the volute tongue is improved, and the volute tongue is arranged axially instead of intersecting line, with the rounded angle of the volute tongue being 2 mm. The structure of the improved volute tongue is shown in Figure 3.

2.3. Grid Generation and Independence Check. During the numerical simulation, the dimensionless head coefficient Ψ was defined as follows:

$$\Psi = \frac{gH}{\left(u_2^2/2\right)}, \tag{1}$$

where g is the acceleration of gravity, H is the head, u_2 is the circumferential velocity at the impeller outlet, $u_2 = \pi D_2 n/60$, D_2 is the impeller outlet diameter, and n is the rotational speed.

Figure 4 shows the relationship between the grid number of the fuel centrifugal pump and the head coefficient. The fuel pump grid was checked for independence with the predicted deviation of the head coefficient less than 1% as the criterion. When the grid number reached 2.4 million, the predicted deviation of head coefficient was less than 1%. After comprehensive consideration, the 2.4 million grid
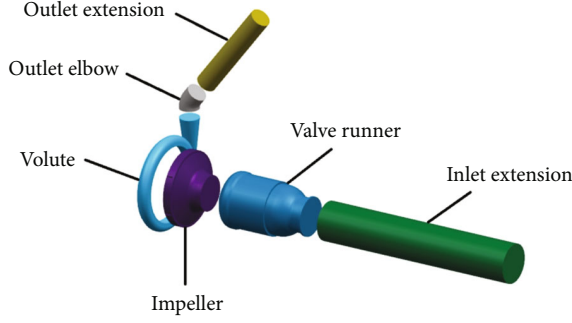
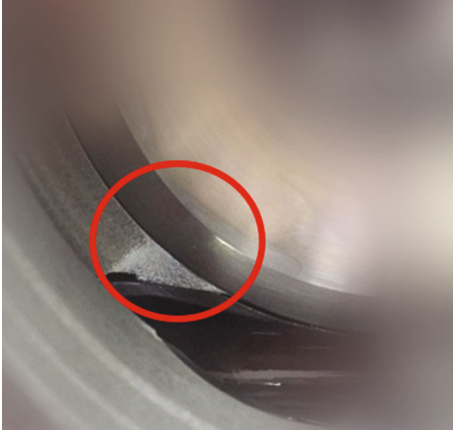FIGURE 1: Computational domain of fuel centrifugal pump.

FIGURE 2: Cavitation damage near the volute tongue.

scheme was selected as the research scheme of this paper. Figure 5 shows the overall grid generation of the fuel centrifugal pump.

2.4. Numerical Calculation Method

2.4.1. Turbulence Model Selection. In order to select a suitable turbulence model for subsequent numerical calculation, the head of the fuel pump under different turbulence models was compared with the test values. Figure 6 shows the schematic diagram of the test, and the measured fuel centrifugal pump is in the red frame. Figure 7 shows the comparison curve of head characteristics in the fuel centrifugal pump under different turbulence models. It can be seen from the figure that the performance curve calculated by the SST model is close to the test performance curve, and the relative error is within 3%.

Figure 8 shows the y^+ value of the improved impeller, and the y^+ value of the grid wall is less than 20, which met the requirement of the turbulence model for wall function during flow field calculation in this paper. Therefore, the SST model was used in the subsequent numerical study.

2.4.2. Cavitation Model Selection. The widely used Zwart-Gerber-Belamri (ZGB) cavitation model was used, which is derived from the Rayleigh-Plesset (R-P) equation.

The Rayleigh-Plesset equation provides the basis for the rate equation controlling steam generation and condensation. The ZGB cavitation model based on the Rayleigh-

Plesset equation was adopted in CFX, wherein r_{ruc} is the volume fraction of cavitation nucleation point, the value is $\alpha_{ruc} = 5 \times 10^{-4}$, and C_{vap} and C_{cond} are the empirical correction coefficients of vaporization and condensation processes, respectively. The values are $C_{vap} = 50$ and $C_{cond} = 0.01$. R_B is the radius of the cavitation nucleation point, and the value is $R_B = 2.0 \times 10^{-6}$ m; the above default values were adopted for cavitation model coefficients.

In the description of the cavitation process, the parameters widely used at present include the cavitation number σ, cavitation margin NPSH, suction specific speed C, and Thoma cavitation coefficient σ_{TH}. In this paper, the dimensionless cavitation number σ was used to describe the inlet condition of fuel centrifugal pump and the possibility of cavitation. The dimensionless cavitation number is related to the inlet pressure and other conditions, which is defined as

$$\sigma = \frac{p_{in} - p_v}{(1/2)\rho u_2{}^2}, \tag{2}$$

where p_{in} is the inlet pressure of the fuel centrifugal pump, p_v is the saturated vapor pressure of the fuel, ρ is the density of the fuel, and u_2 is the reference speed; it refers to the circumferential velocity of the blade outlet diameter in the fuel centrifugal pump, and the circumferential velocity u_2 is calculated by

$$u_2 = \frac{\pi n D_2}{60}, \tag{3}$$

where n is the rotational speed of the fuel centrifugal pump and D_2 is the impeller outlet diameter.

2.4.3. Boundary Condition Setting. The inlet boundary condition was set as pressure inlet, the initial fuel volume fraction was set as 1, and vapor volume fraction was set as 0; the outlet boundary condition is mass flow rate, and the mass flow rate under the design flow rate Q_d is 6.31 kg/s. The solid wall boundary condition is no slip wall, and the flow field wall was set as a smooth wall. In the transient calculation, the flow field is calculated once every 2° of impeller rotation, and the time step is 1.26263×10^{-5} s. The total number of turns is calculated 10 times, and the total time is 0.02727 s; the data in a stable period was selected for analysis.

2.4.4. Medium Property Setting. The working medium is high temperature fuel (132°C), and its main parameters are shown in Table 1.

3. Results and Analysis

3.1. Influence of the Volute Tongue Shape on Cavitation Performance of Fuel Centrifugal Pump. Since the main purpose of the improvement of the volute tongue shape is to improve the cavitation performance of the aviation fuel centrifugal pump, it is necessary to select the cavitation distribution as the analysis content. The critical cavitation number σ_c was defined as the corresponding cavitation number

(a) Original volute tongue   (b) Improved volute tongue
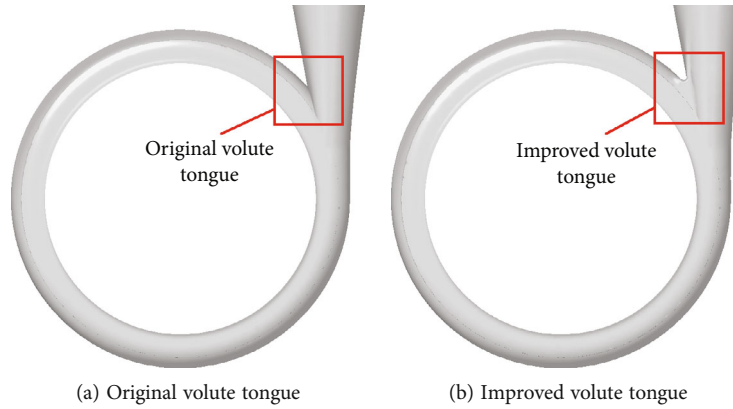
FIGURE 3: Structure of the improved volute tongue.
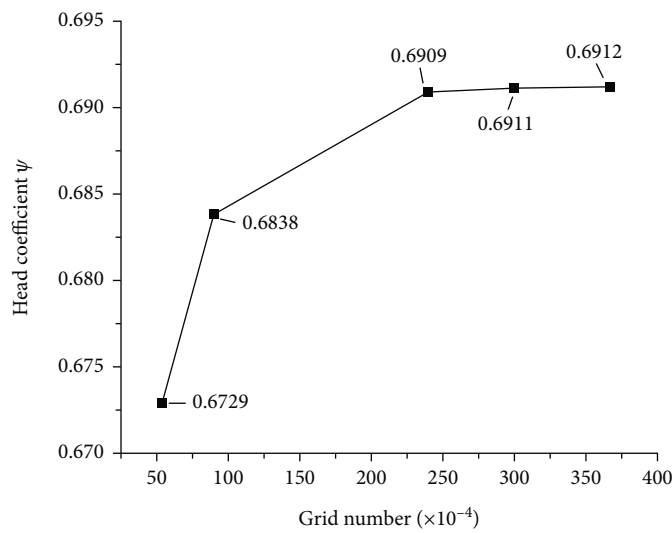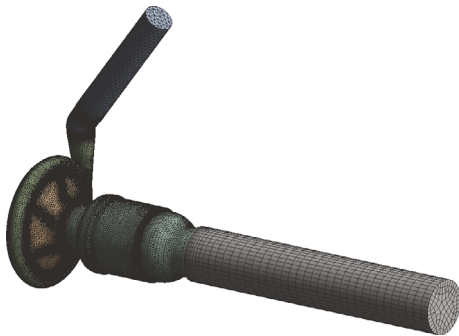

FIGURE 4: Grid independence check.

FIGURE 5: Grid generation of fuel centrifugal pump.

when the head coefficient decreases by 3%. Table 2 shows the comparison of the critical cavitation number σ_c between the original scheme and the improved scheme. The critical cavitation number of the improved volute tongue was reduced compared with the original scheme. Under 0.8 Q_d, 1.0 Q_d, and 1.2 Q_d, the critical cavitation number of the improved volute tongue was reduced by 2.2%, 4.0%, and

7.4%, respectively, compared with the original scheme. Therefore, the improved volute tongue improved the cavitation performance of the fuel centrifugal pump.

3.2. Analysis of Cavitation Occurrence in the Volute Tongue Region. In order to explore the cavitation occurrence in the volute tongue region of the fuel centrifugal pump, the cavitation distribution of three flow rates (0.8 Q_d, 1.0 Q_d, and 1.2 Q_d) that the fuel centrifugal pump operates regularly under the original scheme was selected for numerical analysis.

Figure 9 shows the change of cavitation distribution with the cavitation number in the original fuel centrifugal pump under 0.8 Q_d, where the figures show the isosurface region of cavitation volume fraction α_v of 0.1. When the cavitation number σ is 0.27, the original fuel centrifugal pump generated a small amount of cavitation at the leading edge of the blade. When the cavitation number $\sigma = 0.18$, the cavitation at the leading edge of the blade increased, and at the same time, the cavitation appeared on the back of the inlet extended blade, and a small amount of cavitation appeared on the flow passage hub near the volute tongue. When the
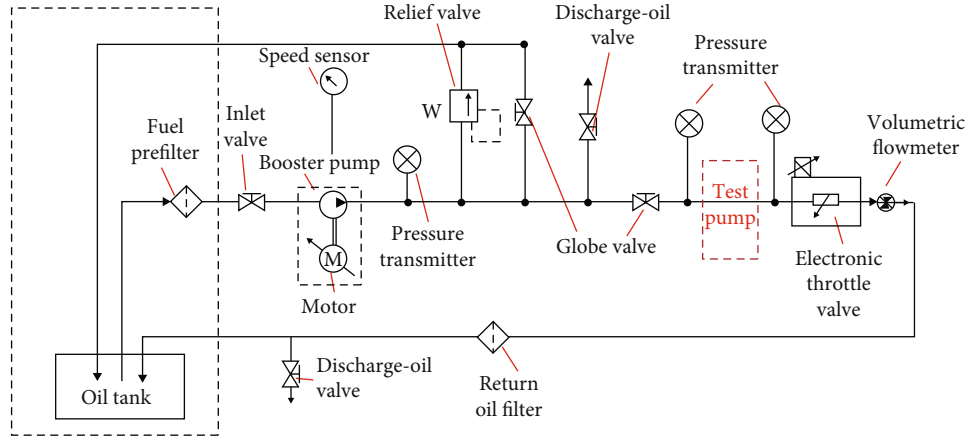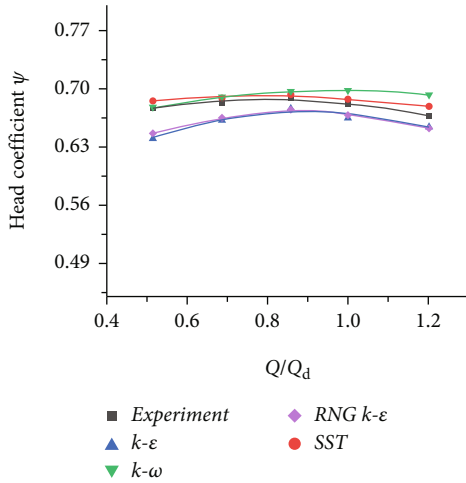
FIGURE 6: Schematic diagram of the test.

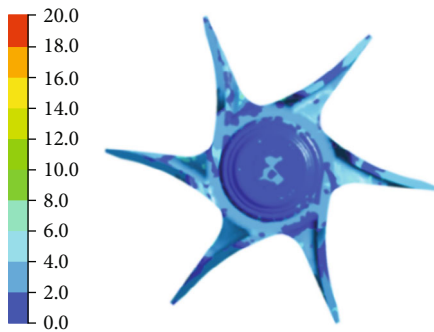FIGURE 7: Comparison curve of head characteristics in the fuel centrifugal pump.

TABLE 1: Parameters of aviation fuel medium.

Physical property	Liquid phase	Gas phase
Molar mass (kg/m^3)	167.31	
Isobaric specific heat capacity (J/(kg·K))	2090	2571
Density (kg/m^3)	780	7.1
Dynamic viscosity (kg/(m^2·s))	0.0024	7×10^{-6}
Surface tension coefficient (N/m)	0.00263257	
Saturated vapor pressure (Pa)	22000	

TABLE 2: Comparison of critical cavitation numbers for pump.

Critical cavitation number σ_c	0.8 Q_d	1.0 Q_d	1.2 Q_d
Original volute tongue	0.045	0.050	0.054
Improved volute tongue	0.044	0.048	0.050

FIGURE 8: y^+ distribution diagram of impeller.

cavitation number σ is 0.14, the cavitation distribution area on the back and root of the blade slightly increased. When the cavitation number σ is 0.10, the cavitation distribution area on the back of the inlet extended blade increased further and gradually extended and developed towards the downstream flow passage. When the cavitation number σ is 0.05, the cavitation distribution area from the extended

blade to the root of the blade was more continuous, and the cavitation distribution area continued to increase. At the same time, the cavitation at the inlet of the impeller is mainly distributed on the suction surface of the extended blade and the spatial torus where it is located. This is due to the complex structure of the inlet valve and the annular flow passage at the end of the valve, which had a certain impact on the flow of the impeller inlet. When extending the inlet edge of the blade to improve the cavitation performance of the pump, the extension of the blade made the distance between the inlet edge of the blade and the outlet of the valve smaller, and the influence of the flow direction caused by the structure of the valve flow passage cannot be completely eliminated. There is a large angle between the flow direction and the inlet of the blade, which had a certain impact on the flow pattern at the inlet of the impeller.

Figure 10 shows the change of cavitation distribution with the cavitation number in the original fuel centrifugal pump under 1.0 Q_d, where the figures show the isosurface region of cavitation volume fraction α_v of 0.1. When the cavitation number σ is 0.27, the cavitation in the original fuel centrifugal pump first appeared at the leading edge of the
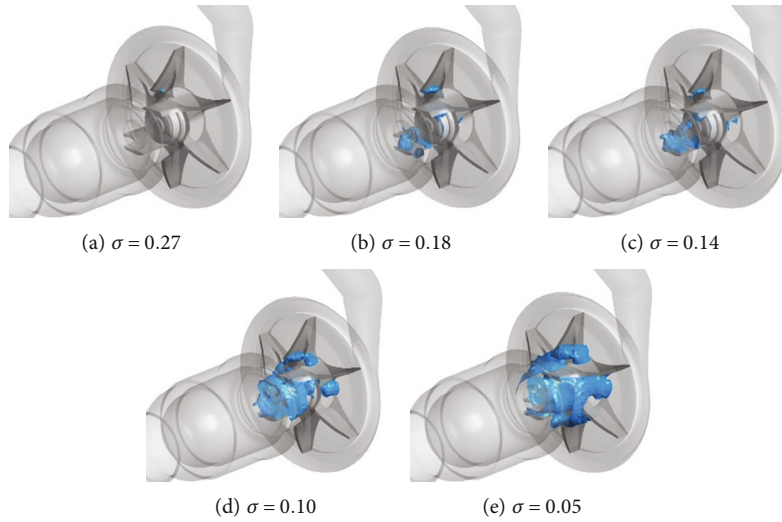
(a) $\sigma = 0.27$ (b) $\sigma = 0.18$ (c) $\sigma = 0.14$

(d) $\sigma = 0.10$ (e) $\sigma = 0.05$

FIGURE 9: Cavitation distributions of the original volute tongue in the fuel centrifugal pump under the 0.8 Q_d.

(a) $\sigma = 0.27$ (b) $\sigma = 0.18$ (c) $\sigma = 0.14$
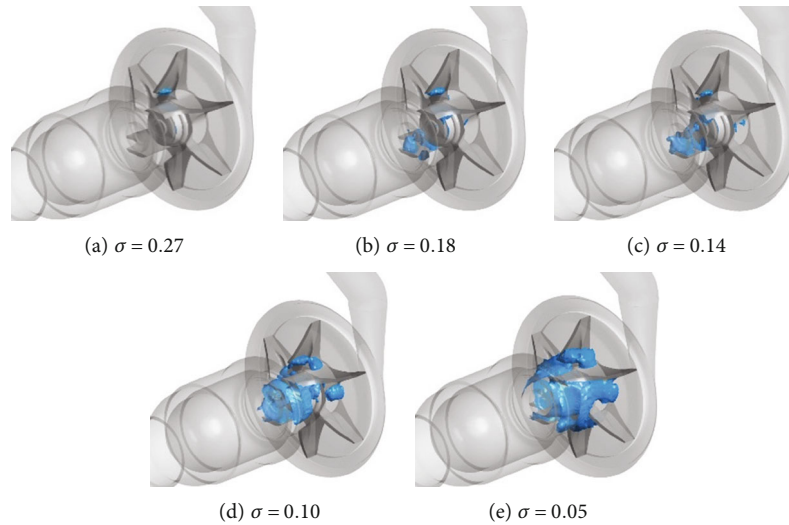
(d) $\sigma = 0.10$ (e) $\sigma = 0.05$

FIGURE 10: Cavitation distributions of the original volute tongue in the fuel centrifugal pump under the 1.0 Q_d.

blade. When the cavitation number σ is 0.18, there was a small amount of cavitation in the impeller, and the cavitation area at the leading edge of the blade increased. At the same time, the cavitation began to appear at the back of the extended blade and the hub of the flow passage near the volute tongue. When the cavitation number σ is 0.14, the cavitation distribution area further increased, and the cavitation at the root of the blade began to appear in other flow passages. With the further decrease of the inlet pressure, when the cavitation number σ is 0.10, the outer edge of the extended blade had a higher dynamic pressure, while the static pressure decreased, resulting in a gradual increase of the cavitation torus of the extended blade and extended downstream to the hub at the root of the impeller. When the cavitation number σ is 0.05, the extended blade cavitation occupied most of the inlet area, but there was relatively little cavitation on the extended blade pressure face. At the same time, the extended blade cavitation area and the blade root cavitation distribution were more continuous.

Figure 11 shows the change of cavitation distribution with the cavitation number in the original fuel centrifugal pump under 1.2 Q_d, where the figures show the isosurface region of cavitation volume fraction α_v of 0.1. When the cavitation number σ is 0.27, the original fuel centrifugal pump generated a small amount of cavitation near the leading edge of the blade, but no obvious cavitation occurred at the root of the blade. When the cavitation number σ is 0.18, the cavitation accumulation area was formed at the hub of the pressure face passage of the extended blade sweeping the volute tongue, and the cavitation began to connect at the leading edge of the blade and the root of the blade. At this time, the cavitation area occurring at the back of the extended blade and the root of the hub was more obvious. When the cavitation number σ is 0.14, the cavitation distribution area increased slightly. When the cavitation number σ is 0.10, the cavitation distribution area at the root of the blade further increased, and a continuous cavitation distribution was formed at the inlet of the impeller. When the cavitation
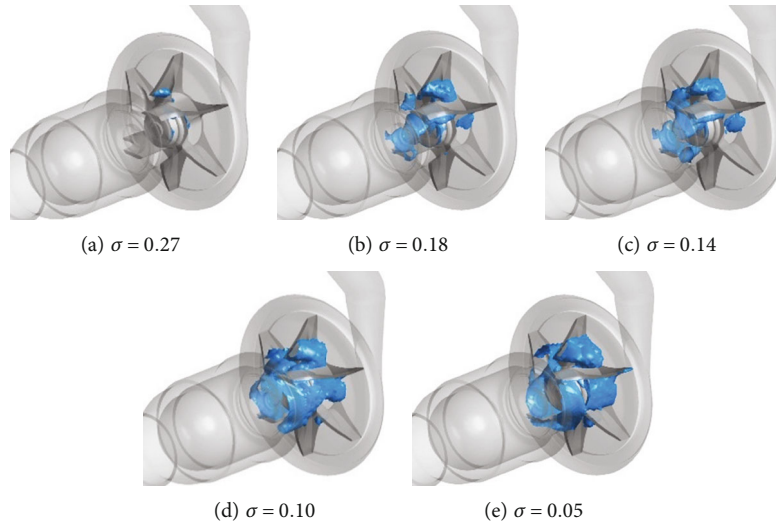
(a) $\sigma = 0.27$ (b) $\sigma = 0.18$ (c) $\sigma = 0.14$

(d) $\sigma = 0.10$ (e) $\sigma = 0.05$

FIGURE 11: Cavitation distributions of the original volute tongue in the fuel centrifugal pump under the 1.2 Q_d.

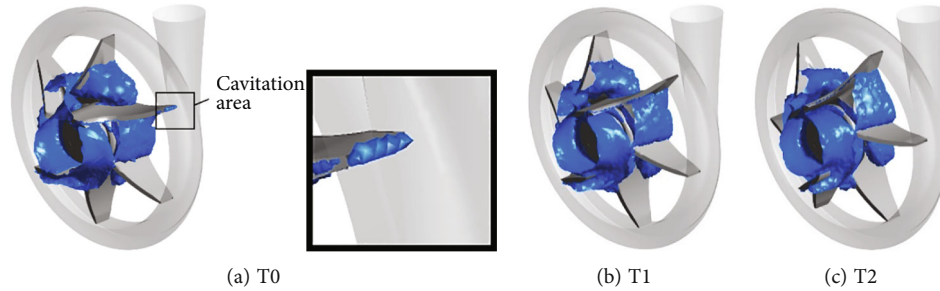

(a) T0   (b) T1   (c) T2

FIGURE 12: Unsteady evolution of cavitation in the original tongue region at σ of 0.05.

number σ is 0.05, cavitation had fully developed and the distribution area of cavitation continued to increase. At the same time, when the blade swept the volute tongue, there was an obvious cavitation accumulation area on the top of the blade, which may cause cavitation damage to the volute tongue wall when passing the volute tongue.

By comparing the changes in cavitation distribution with the cavitation number under the three flow rates, it can be seen that, as the cavitation number decreased, cavitation began to appear at the root of the blade and the suction surface of the extended blade and gradually increased. The cavitation in the volute tongue region of the fuel centrifugal pump occurred at 1.2 Q_d; when the blade swept the volute tongue, the cavitation gathered at the top of the blade. Therefore, the cavitation characteristics of the fuel centrifugal pump in the improved scheme and the original scheme were only compared and analyzed when the cavitation number σ is 0.10 and 0.05 under 1.2 Q_d.

3.3. Influence of the Volute Tongue Shape on Cavitation Distribution in the Impeller. When flow rate is 1.2 Q_d and σ is 0.10, the cavitation did not gather at the top of the blade when the blade of the fuel centrifugal pump swept the volute tongue. Therefore, the influence of the improved volute tongue shape on the cavitation distribution in the impeller at σ of 0.05 was analyzed.

Figures 12 and 13 show the cavitation distribution in the volute tongue region of the fuel centrifugal pump under the original scheme and the improved scheme when the cavitation number σ is 0.05, respectively. The figures show the isosurface region of the cavitation volume fraction α_v of 0.1 at the blade outlet before the blade swept the volute tongue. The cavitation distribution of the blade at three positions before the volute tongue (T0), at the volute tongue (T1), and after the volute tongue (T2) was analyzed.

It can be seen from Figure 12 that in the process of the blade sweeping the volute tongue, the cavitation area was formed at the top of the blade in the original scheme. At this time, the blade was in the front of the volute tongue at the intersection line. With the rotation of the impeller, the cavitation accumulation area at the top of the blade had basically disappeared at T1, and the cavitation collapsed from T0 to T1. When the impeller continued to rotate and the blade passed through the volute tongue, the cavitation at the top of the blade completely disappeared.

As can be seen from Figure 13, cavitation in the volute tongue region of the improved scheme was significantly weakened when the blade swept the volute tongue. There was no significant cavitation in the volute tongue region at T0, T1, and T2. Therefore, when matching the improved
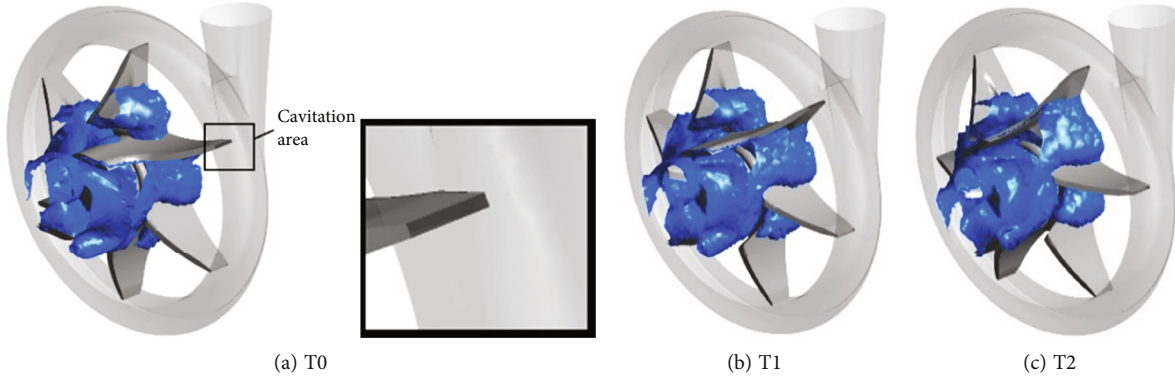
(a) T0   (b) T1   (c) T2

FIGURE 13: Unsteady evolution of cavitation in the improved tongue region at σ of 0.05.

(a) T0   (b) T1   (c) T2
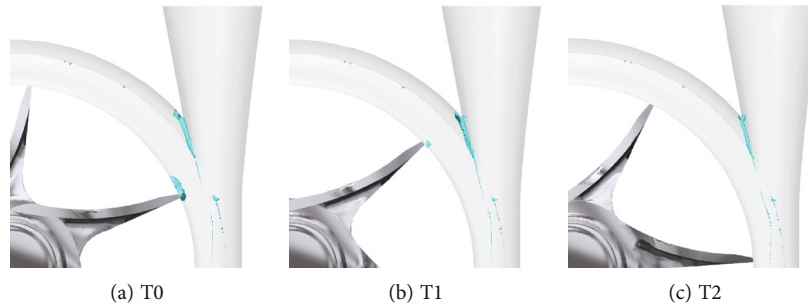
FIGURE 14: Unsteady evolution of vortex core near the original volute tongue region at the cavitation number of 0.10.

volute tongue and the impeller, the cavitation in the volute tongue region will be significantly weakened, which will improve the cavitation damage to the volute tongue wall.

3.4. Influence of the Volute Tongue Shape on Vortex Core Distribution in the Volute.

On the other hand, because the cavitation flow will produce local bubbles, which will affect the flow of the fluid and form vortex core, the analysis of vortex core can also reflect the energy loss and cavitation performance changes in the aviation fuel centrifugal pump. In order to explore the influence of the axial rounding shape on the flow field of the fuel pump, combined with the occurrence of cavitation in the volute tongue region, the evolution process of the vortex core at T0, T1, and T2 was emphatically analyzed.

Figure 14 shows the distribution of the vortex core near the volute tongue of the fuel centrifugal pump blade in the original scheme at the cavitation number σ of 0.10, and the figure shows the contour surface of vortex core Q_c of $8 \times 10^7\,S^{-2}$. It can be seen from Figure 14 that the original scheme had a large vortex core distribution area along the intersecting line of the volute tongue, which may have a greater impact on the flow field when the blade swept the volute tongue. A long vortex core was formed at the blade outlet when the blade is close to the volute tongue. The volume of the vortex core was the largest at T1. With the rotation of the impeller, the vortex core distribution area on the volute tongue wall and the impeller outlet decreased, especially the vortex core volume at the impeller outlet decreased more significantly. The vortex core distribution area at the

impeller outlet had disappeared at T3, and the contour surface of the vortex core in the volute tongue region was mainly distributed at the volute tongue of the intersecting line, indicating that the separation vortex caused by the high-speed shear flow on the volute tongue wall always existed in the process of blade sweeping the volute tongue, which had a major impact on the flow field near the volute tongue.

Figure 15 shows the vortex core distribution near the volute tongue of the fuel centrifugal pump blade under the improved scheme at the cavitation number σ of 0.10. It can be seen from Figure 15 that the distribution of the vortex core in the volute tongue region of the improved scheme was significantly reduced compared with the original scheme. The volume distribution of the vortex core at the outlet of the impeller was very small at T0, while the improved volute tongue wall did not form an obvious vortex structure. With the rotation of the impeller, the vortex core at the outlet of the impeller completely disappeared at T1 and T2, and the separation vortex on the volute tongue wall was effectively suppressed.

By comparing the changes of the vortex core in different schemes at the cavitation number σ of 0.10, it can be seen that the original scheme had a larger vortex core distribution area in the volute tongue of the intersecting line, and the vortex core did not disappear as the impeller passed through the volute tongue, while the improved volute tongue had a significant control effect on the separation vortex on the volute tongue surface, avoiding the influence of the separation vortex on the flow field.
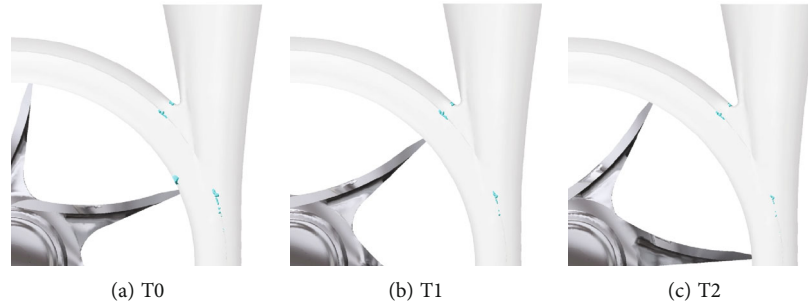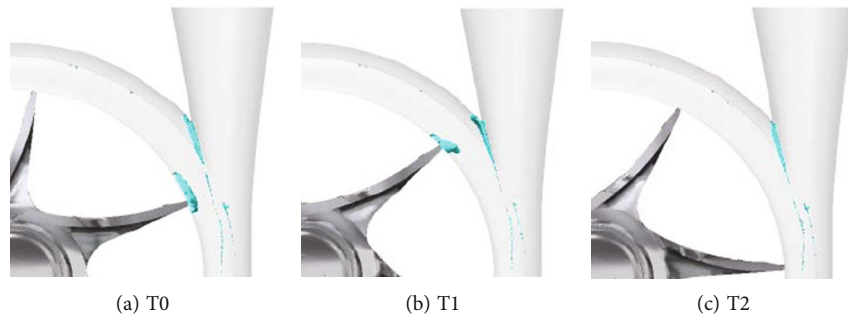
(a) T0   (b) T1   (c) T2

FIGURE 15: Unsteady evolution of vortex core near the improved volute tongue region at the cavitation number of 0.10.

(a) T0   (b) T1   (c) T2

FIGURE 16: Unsteady evolution of vortex core near the original volute tongue region at the cavitation number of 0.05.
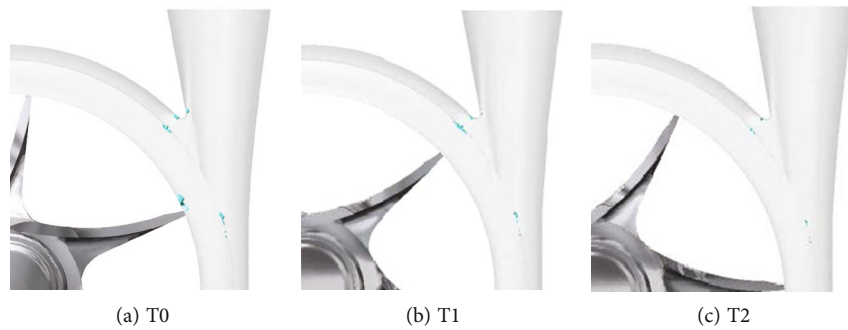

(a) T0   (b) T1   (c) T2

FIGURE 17: Unsteady evolution of vortex core near the improved volute tongue region at the cavitation number of 0.05.

Figure 16 shows the vortex core distribution near the volute tongue of the fuel centrifugal pump blade under the original scheme at the cavitation number σ of 0.05. As can be seen from Figure 16, the separation vortex core on the volute tongue wall of the original scheme did not change significantly with the rotation of the impeller. The volume of the vortex core at the outlet of the impeller was larger at T0; the vortex core at the impeller outlet decreased at T1 and disappeared at T3.

Figure 17 shows the vortex core distribution near the volute tongue of the fuel centrifugal pump blade under the improved scheme at the cavitation number σ of 0.05. As can be seen from Figure 17, the separation vortex on the volute tongue wall of the improved scheme was effectively suppressed, indicating that the improved volute tongue had a more obvious weakening effect on the separation vortex on the volute tongue wall. The volume of the vortex core

at the outlet of the impeller was reduced compared with the original scheme at T0, and it completely disappeared at T1 and T2.

By comparing the unsteady changes of the vortex core in different schemes at the cavitation number σ of 0.05, it can be seen that there is an obvious separation vortex on the wall of the volute tongue in the original scheme. When the blade and the volute tongue are in different relative positions, the separation vortex core distribution was not significantly affected. The results show that the separation vortex formed by high-speed shear flow in the process of the blade sweeping the volute tongue was not obviously affected by the relative position of the blade and the volute tongue. The improved scheme did not form an obvious vortex core on the volute tongue wall, indicating that the generation of wall separation vortex was effectively suppressed in the axial direction at a low cavitation number. At the same time,
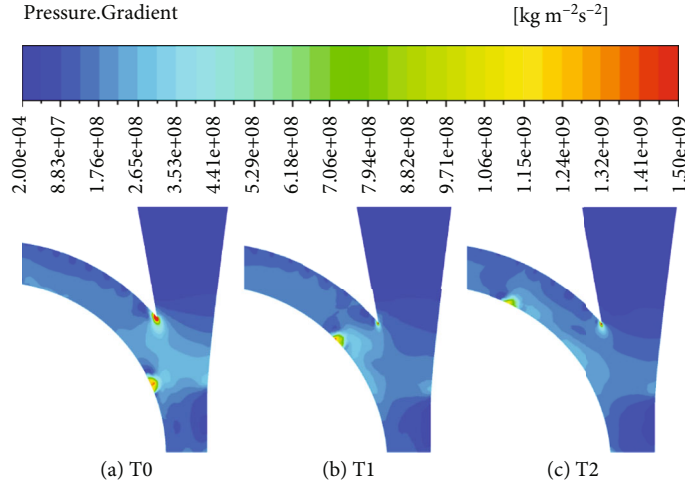
Figure 18: Pressure gradient distribution near the original volute tongue region at the cavitation number of 0.10.
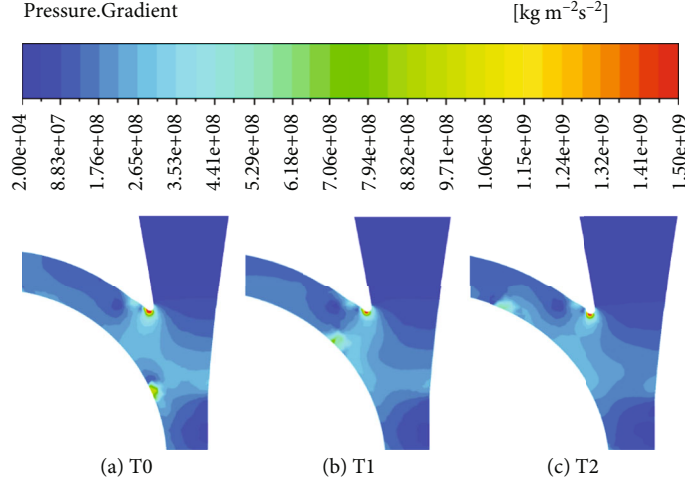

Figure 19: Pressure gradient distribution near the improved volute tongue region at the cavitation number of 0.10.

when the blade approached the volute tongue, the vortex core formed in front of the diaphragm and disappeared in the process of gradually approaching the volute tongue. After volute tongue swept volute tongue, there was no new vortex core formed at the top of the blade after the blade swept the volute tongue, which indicated that the tip vortex formed in front of the volute tongue during the dynamic process of the blade sweeping the volute tongue and then gradually disappeared. The volume of the vortex core at the top of the blade in the original scheme was larger at T0 and T1, while the volume of the vortex core at the top of the blade in the improved scheme was significantly smaller than that in the original scheme at low cavitation number.

By comparing the distribution of vortex core under different cavitation numbers, it can be found that when the cavitation number σ is 0.10, the volume of separated vortex core distributed along the volute tongue wall in the improved scheme was significantly reduced compared with that in the original scheme, and the distribution area

of vortex core at the top of the blade was also reduced during the blade sweeping the volute tongue. When the cavitation number σ is 0.05, the separation flow generated on the volute tongue wall in the original scheme was not significantly affected by the reduction of the cavitation number. In the improved scheme, the separation vortex core on the volute tongue wall was not significantly affected by the reduction of the cavitation number, but the volume of the vortex core at the top of the blade increased with the reduction of the cavitation number. The distribution area of the vortex core at the top of the blade in both schemes increased at T0, but the vortex core in the improved scheme was obviously smaller than that in the original scheme. In general, the axial arrangement of the rounded volute tongue weakened the separation vortex on the volute tongue wall, and the vortex core region at the top of the blade was reduced, which improved the flow field in the volute tongue region and facilitated the discharge of the fluid in the impeller through the diffusion section.
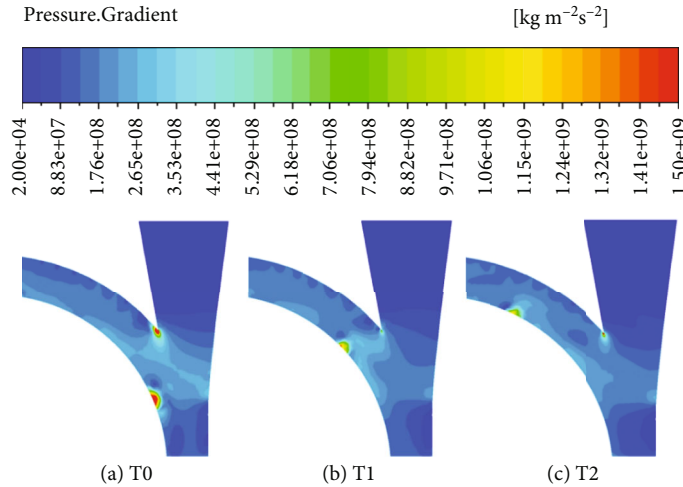
FIGURE 20: Pressure gradient distribution near the original volute tongue region at the cavitation number of 0.05.
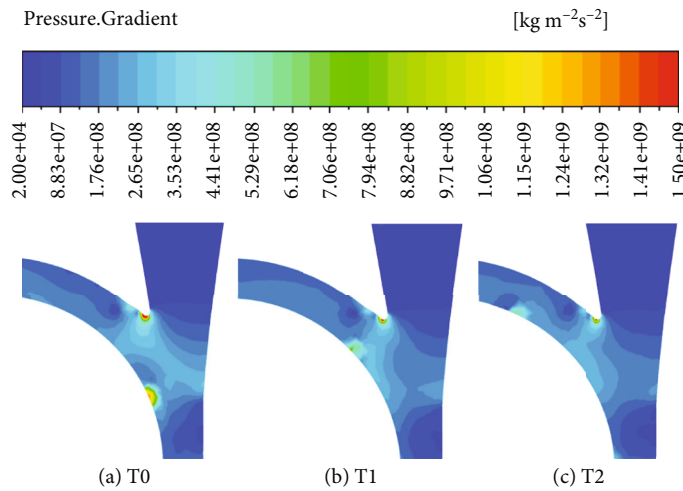

FIGURE 21: Pressure gradient distribution near the improved volute tongue region at the cavitation number of 0.05.

3.5. Influence of the Volute Tongue Shape on the Volute Pressure Gradient.

Since cavitation is often accompanied by strong vortex motion, the internal pressure in the vortex core region is lower than that in the circulation region, and a larger pressure gradient is formed under the action of the vapor-liquid interface in the cavitation region. Therefore, combined with the cavitation occurrence condition in the volute tongue region, the pressure gradient in the volute tongue region was analyzed.

Figure 18 shows the pressure gradient distribution in the original volute tongue region of the fuel centrifugal pump at the cavitation number σ of 0.10. It can be seen from Figure 18 that in the process of the blade sweeping the volute tongue, the original scheme formed a large pressure gradient distribution area at the location of flow separation on the volute tongue wall and at the top of the blade, respectively. When the local pressure is lower than the saturated steam pressure, it is easy to cause cavitation at this location. High pressure gradient region on the volute tongue wall and the top of the blade was significant at T0. With the rotation of
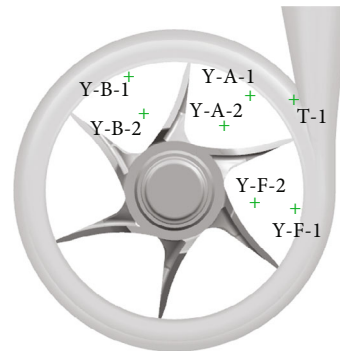

FIGURE 22: Monitoring points of impeller passage and tongue region.

the impeller, the pressure gradient gradually decreased at T1 and T2.

Figure 19 shows the pressure gradient distribution in the improved volute tongue region of the fuel centrifugal pump at the cavitation number σ of 0.10. It can be seen from

(a) Original volute tongue
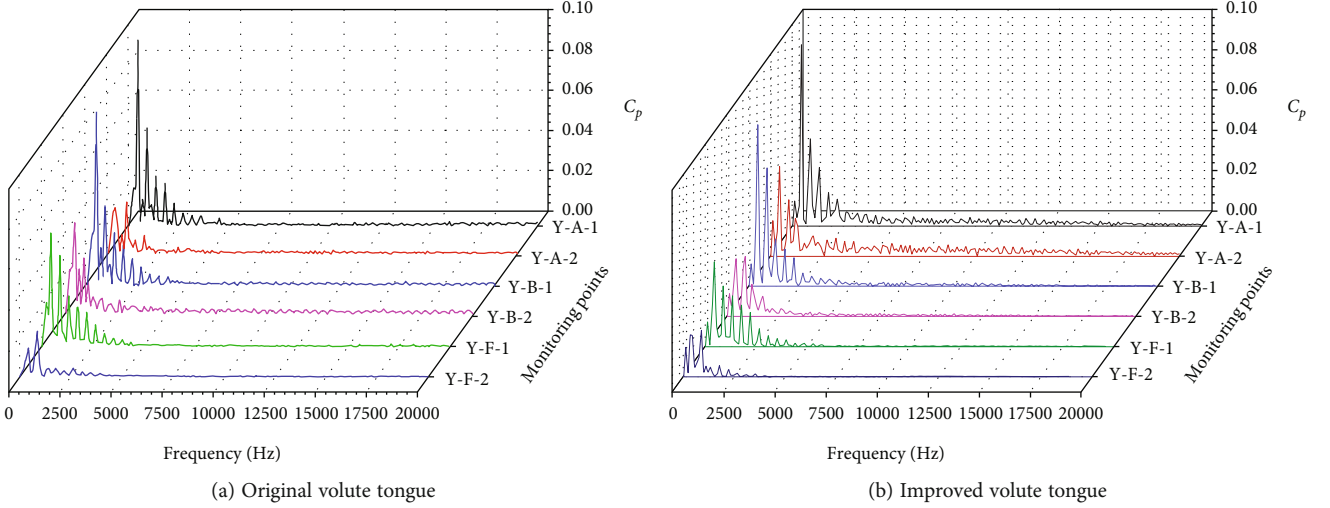

(b) Improved volute tongue

FIGURE 23: Frequency domain distribution of pressure pulsation at monitoring point of impeller at the cavitation number of 0.10.

Figure 19 that the pressure gradient of the improved scheme was reduced compared to the original scheme at T0. With the rotation of the impeller, the pressure gradient is gradually reduced when the blade is close to and far from the volute tongue.

Figures 20 and 21, respectively, show the pressure gradient changes of the volute tongue region of the fuel centrifugal pump under the original scheme and the improved scheme at the cavitation number σ of 0.05. It can be seen from Figure 20 that the pressure gradient of the original scheme on the volute tongue wall and the top of the blade was relatively high. With the rotation of the impeller, the pressure gradient gradually reduced at T1 and T2. It can be seen from Figure 21 that compared with the original scheme, the pressure gradient of the improved scheme was reduced. At T1 and T2, the pressure gradient gradually reduced.

By comparing the pressure gradient distribution at the cavitation number of 0.10 and 0.05, it can be seen that under 1.2 times of flow rate, the pressure gradient at the top of the blade in the volute tongue region was reduced by modifying the shape of the volute tongue, indicating that the improvement of cavitation in the volute tongue region had a certain influence on the flow field vortex and the vapor-liquid interface, which reduced the pressure gradient.

3.6. Influence of the Volute Tongue Shape on Pressure Pulsation Characteristics.
In order to explore the characteristics of pressure pulsation in the internal flow field of the fuel centrifugal pump under 1.2 Q_d, monitoring points were arranged in the impeller and the volute tongue region, respectively. The rotation speed of the impeller is 26400 r/min, its axial frequency is 440 Hz, and its blade frequency is 2640 Hz. The pressure pulsation coefficient C_p was introduced in the analysis.

$$C_p = \frac{P - \bar{P}}{0.5\rho u^2}, \qquad (4)$$

where P is the static pressure at a certain time, $\bar{P}$ is the average static pressure during a rotation of the impeller, and u is the circumferential velocity of the location of each monitoring point.

Since the impeller has two symmetrical extended blades, each flow passage is not completely symmetrical. Therefore, three flow passages were selected to set monitoring points, which are located in the middle section of the impeller outlet. Monitoring points Y-A-1 and Y-A-2 were set in channel A, Y-B-1 and Y-B-2 were set in channel B, and Y-F-1 and Y-F-2 were set in channel F. The monitoring points in the impeller rotated with the computational domain of the impeller. At the same time, monitoring point T-1 was set in the volute tongue region. The pressure pulsation monitoring points are shown in Figure 22.

Figure 23 shows the frequency domain of pressure pulsation at the monitoring point of the impeller passage in the fuel centrifugal pump at the cavitation number σ of 0.10. As can be seen from Figure 23, the main frequency of Y-A-1, Y-A-2, Y-B-1, Y-B-2, Y-F-1, and Y-F-2 in the flow passage of the improved scheme all appeared in the axial frequency, and the maximum pressure pulsation amplitude appeared near the outlet of the impeller passage. The amplitude of the pressure pulsation coefficient at the outlet monitoring points of different flow passages A, B, and F was Y-A-1 > Y-B-1 > Y-F-1, while the amplitude of the flow passage monitoring points Y-A-2, Y-B-2, and Y-F-2 was lower than that at the outlet. The difference compared with the original scheme is that the amplitude of the flow passage monitoring points was reduced.

Figure 24 shows the frequency domain of pressure pulsation at the monitoring point of the impeller passage in the fuel centrifugal pump at the cavitation number σ of 0.05. The main frequency of pressure pulsation in the improved scheme is the axial frequency of the impeller. The maximum amplitude of pressure pulsation appeared at monitoring points Y-A-1, Y-B-1, and Y-F-1 near the impeller outlet. The pressure pulsation amplitude is ordered as Y-A-1 > Y-B-1 > Y-F-1. Different from the original scheme, the amplitude of pressure pulsation
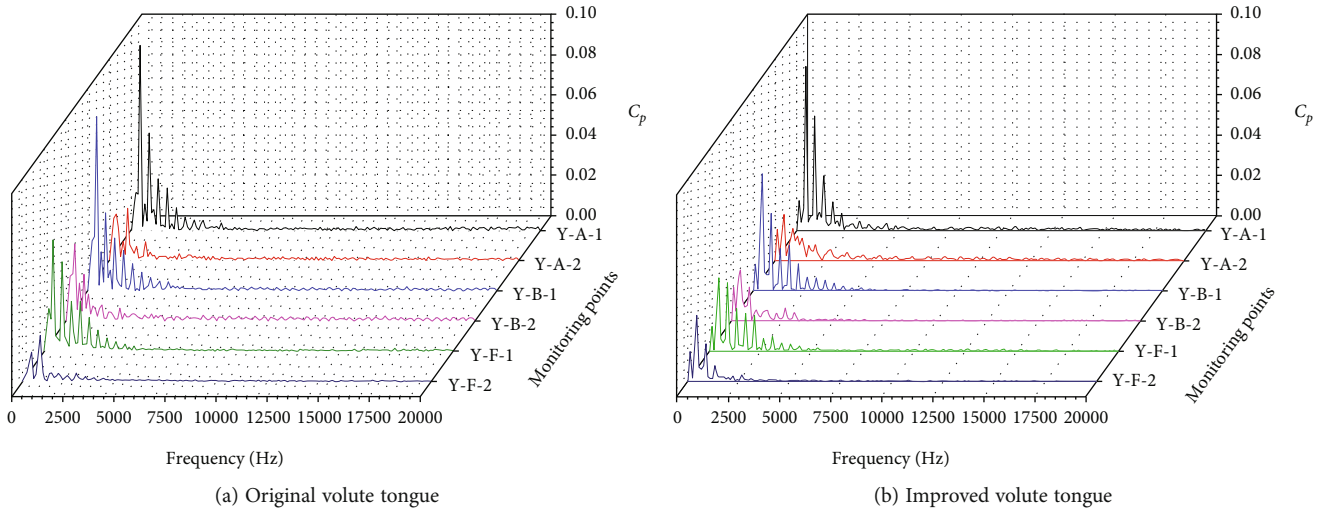
(a) Original volute tongue

(b) Improved volute tongue

Figure 24: Frequency domain distribution of pressure pulsation at monitoring point of impeller at the cavitation number of 0.05.

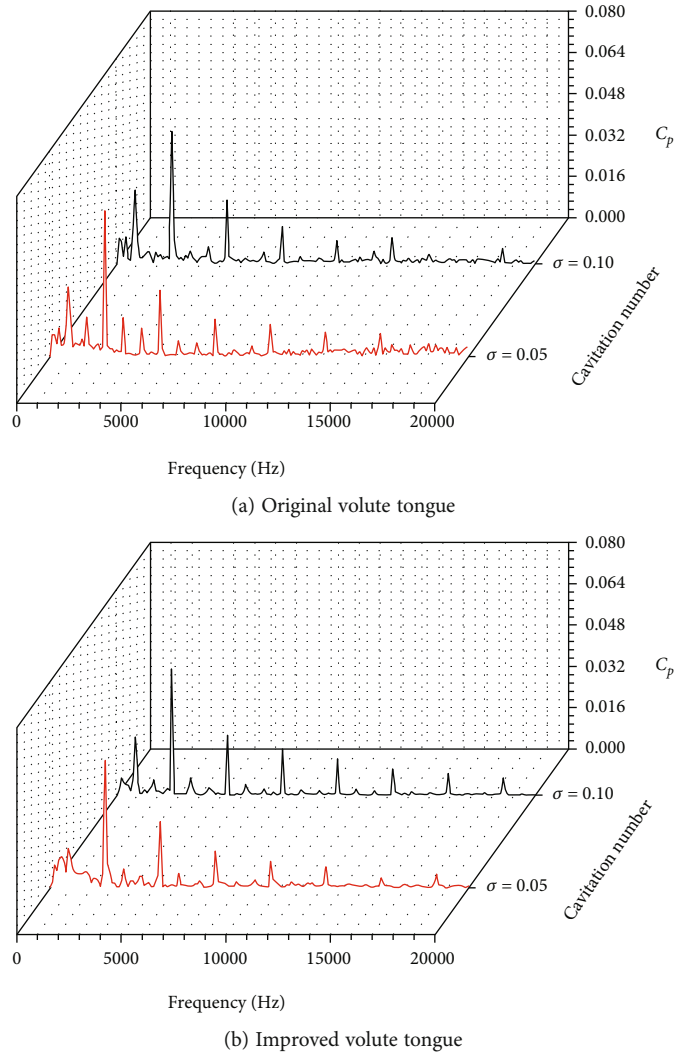(a) Original volute tongue

(b) Improved volute tongue

Figure 25: Frequency domain distribution of pressure pulsation at monitoring point of volute tongue.

was relatively reduced, and the maximum amplitude of pressure pulsation at the monitoring points in the flow passage was reduced by 11.3% compared with the original scheme.

Figure 25 shows the pressure pulsation frequency distribution of monitoring point T-1 at the volute tongue of the fuel centrifugal pump. The main frequency of the pressure pulsation at monitoring point T-1 in the improved scheme was blade frequency (2640 Hz), and the amplitude of the main frequency slightly increased with the reduction of the cavitation number ($\sigma = 0.05$). Different from the original scheme, when the cavitation number σ is 0.05, the doubling of the axial frequency of the monitoring point T-1 pressure pulsation spectrum disappeared, which may be related to the weakening of cavitation in the volute tongue region.

Combined with the improvement of the cavitation in the volute tongue region with the improved volute tongue at a low cavitation number under 1.2 Q_d, it is shown that the doubling of the axial frequency of the monitoring point T-1 pressure pulsation in the volute tongue region is related to the cavitation flow field in the volute tongue region.

4. Conclusion

Aiming at the cavitation in the volute tongue region of the fuel centrifugal pump under 1.2 times of flow rate, the influence of improved volute tongue shape on the fuel pump cavitation under this condition was studied, and compared with the original scheme, the main conclusions are as follows:

(1) The critical cavitation number of the improved scheme is reduced by 2.2%, 4.0%, and 7.4% compared with the original scheme under 0.8 Q_d, 1.0 Q_d, and 1.2 Q_d, and the cavitation performance is further improved

(2) At the low cavitation number of 1.2 times of flow rate, the axial volute tongue shape effectively suppressed the formation of cavitation in the volute tongue region

(3) In the improved scheme, the volume of the vortex core is obviously reduced on the volute tongue wall and at the top of the blade when the blade sweeps the volute tongue of the fuel centrifugal pump, and the pressure gradient in the volute tongue region is reduced

(4) In the improved scheme, the main frequency of pressure pulsation at monitoring points Y-A-1, Y-A-2, Y-B-1, Y-B-2, Y-F-1, and Y-F-2 of impeller passage of fuel centrifugal pump is the axial frequency (440 Hz). The main frequency of pressure pulsation at monitoring point T-1 in the volute tongue region is blade frequency (2640 Hz), and the amplitude of the pressure pulsation is lower than that of the original scheme. When the cavitation number σ is 0.05, the doubling of the axial frequency amplitude of the pressure pulsation at monitoring point T-1 of the volute tongue in the improved scheme is significantly reduced

References

[1] K. Wang, R. X. Gong, G. Z. Luo, Y. Wang, H. L. Liu, and H. Wang, "Cavitation characteristics of high-speed fuel centrifugal pump," *Journal of Propulsion Technology*, vol. 43, no. 10, article 210521, 2022.

[2] M. J. Kim, H. B. Jin, and W. J. Chung, "A study on prediction of cavitation for centrifugal pump," *World Academy of Science*, vol. 6, no. 12, pp. 612–617, 2012.

[3] X. Wang, Y. Wang, H. Liu, Y. Xiao, L. Jiang, and M. Li, "A numerical investigation on energy characteristics of centrifugal pump for cavitation flow using entropy production theory," *International Journal of Heat and Mass Transfer*, vol. 201, article 123591, Part 2, 2023.

[4] H. Zhu, N. Qiu, C. Wang et al., "Prediction of cavitation evolution and cavitation erosion on centrifugal pump blades by the DCM-RNG method," *Scanning*, vol. 2021, Article ID 6498451, 12 pages, 2021.

[5] J. Zhang, X. P. Chen, C. M. Su, and Z. Zhao, "Study on the influence of blade perforation near inlet edge on cavitation and turbulent kinetic energy of centrifugal pump," *Fluid Machinery*, vol. 49, no. 7, pp. 14–19, 2020.

[6] G. Mousmoulis, I. Kassanos, G. Aggidis, and I. Anagnostopoulos, "Numerical simulation of the performance of a centrifugal pump with a semi-open impeller under normal and cavitating conditions," *Applied Mathematical Modelling*, vol. 89, no. 3, pp. 1814–1834, 2021.

[7] X.'a. Zhao, B. Huang, T. Chen, G. Wang, D. Gao, and J. Zhao, "Numerical simulations and surrogate-based optimization of cavitation performance for an aviation fuel pump," *Journal of Mechanical Science and Technology*, vol. 31, no. 2, pp. 705–716, 2017.

[8] W. J. Wang, "Research status and prospect of centrifugal aviation fuel pump," *Fluid Machinery*, vol. 48, no. 10, pp. 59–63, 2020.

[9] J. B. Hu, R. Y. Xue, H. L. Liu, K. Wang, and X. Lu, "Hydraulic optimization and experimental measurement of low specific speed centrifugal fire pump," *Journal of Applied Fluid Mechanics*, vol. 15, no. 5, pp. 1477–1489, 2022.

[10] K. Wang, C. Wang, C. Xia, H. Liu, and Z. Zhang, "Experimental measurement of cavitation-induced vibration characteristics in a multi-stage centrifugal pump," *Journal of Chemical Engineering of Japan*, vol. 51, no. 3, pp. 203–209, 2018.

[11] Y. Liu, X. Li, W. Wang, L. Li, and Y. Huo, "Numerical investigation on the evolution of forces and energy features in

thermo-sensitive cavitating flow," *European Journal of Mechanics - B/Fluids*, vol. 84, pp. 233–249, 2020.

[12] Z. Chen, S. Yang, X. Li, Y. Li, and L. Li, "Investigation on leakage vortex cavitation and corresponding enstrophy characteristics in a liquid nitrogen inducer," *Cryogenics*, vol. 129, article 103606, 2023.

[13] X. Li, Y. Liu, Z. Zhu, P. Lin, and L. Li, "Boundary vorticity analysis and shedding dynamics of transient cavitation flow around a twisted hydrofoil," *Journal of Fluids Engineering*, vol. 143, no. 7, article 071501, 2021.

[14] X. Li, Z. Jiang, Z. Zhu, Q. Si, and Y. Li, "Entropy generation analysis for the cavitating head-drop characteristic of a centrifugal pump," *Proceedings of the Institution of Mechanical Engineers, Part C: Journal of Mechanical Engineering Science*, vol. 232, no. 24, pp. 4637–4646, 2018.

[15] F. Visser, "Some user experience demonstrating the use of CFX-TASCflow computational fluid dynamics for cavitation inception (NPSH) analysis and head performance prediction of centrifugal pump impellers," in *ASME Fluids Engineering Division Summer Meeting*, USA: New Orleans, Louisiana, 2001.

[16] B. Schiavello and F. C. Visser, "Pump Cavitation – Various NPSHR Criteria, NPSH Margins, and Impeller Life Expectancy," in *International Pump Users Symposium*, USA: Houston, Texas, 2007.

[17] J. Li, H. C. Li, W. C. Wang, and Y. Wang, "Multi-objective optimization design and simulation for fuel centrifugal pump," *Journal of Propulsion Technology*, vol. 42, no. 3, pp. 666–674, 2021.

[18] Y. Wang, H. C. Li, S. H. Wang, and J. Li, "Simulation on transient flow characteristics for an aero-fuel centrifugal pump with combination blades under condition of low flowrate," *Journal of Propulsion Technology*, vol. 43, no. 7, article 200516, 2022.

[19] P. Dupont, "Numerical prediction of cavitation — improving pump design," *World Pumps*, vol. 2001, no. 422, pp. 26–28, 2001.

[20] J. Li, X. Wang, Y. Wang, W. Wang, B. Chen, and X. Chen, "Effects of a combination impeller on the flow field and external performance of an aero-fuel centrifugal pump," *Energies*, vol. 13, no. 4, p. 919, 2020.